Volume 7 | Number 5 | 7 February 2015 | Pages 1513–2130

Nanoscale

www.rsc.org/nanoscale

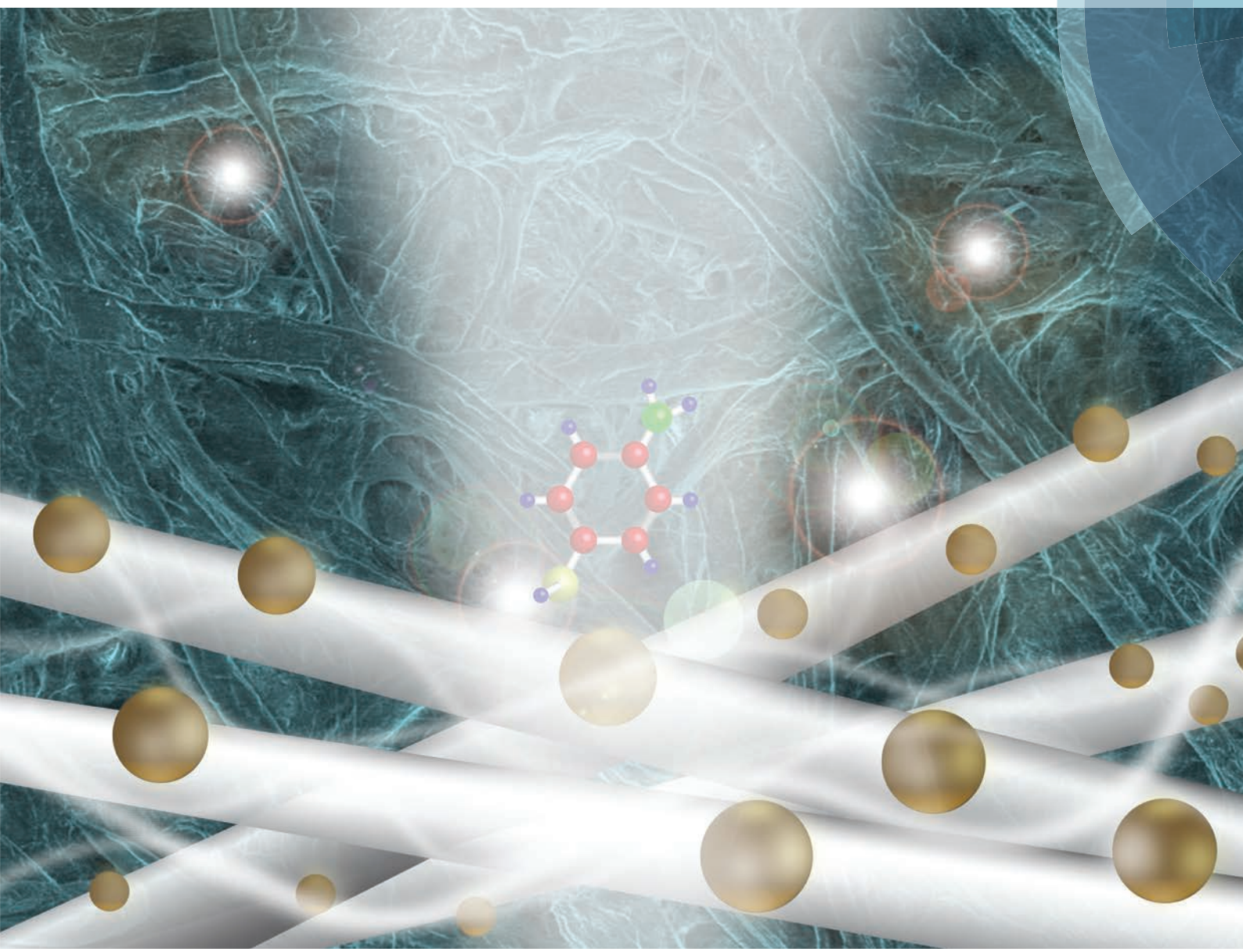

ISSN 2040-3364

ROYAL SOCIETY OF CHEMISTRY

PAPER
Hsuen-Li Chen *et al.*
Single-shot laser treatment provides quasi-three-dimensional paper-based substrates for SERS with attomolar sensitivity

NCNST

Nanoscale

PAPER

Cite this: *Nanoscale*, 2015, **7**, 1667

Single-shot laser treatment provides quasi-three-dimensional paper-based substrates for SERS with attomolar sensitivity†

Chen-Chieh Yu, Sin-Yi Chou, Yi-Chuan Tseng, Shao-Chin Tseng, Yu-Ting Yen and Hsuen-Li Chen*

Received 6th September 2014,
Accepted 15th October 2014

DOI: 10.1039/c4nr05178e

www.rsc.org/nanoscale

In this study, an eco-friendly and ultrasensitive paper substrate is developed for surface-enhanced Raman scattering (SERS) with performance approaching single molecule detection. By exploiting the laser-induced photothermal effect, paper fibrils with hybrid micro- and nanostructures can facilitate the formation of highly dense metal nanoparticles (NPs) after a single shot of laser illumination. Metal films deposited on the paper substrates feature discontinuous morphologies, with the fragments acting as multiple nucleation sites. Because thermal conductivity is low on the broken films and the underlying paper fibrils, the incident energy is absorbed efficiently. Moreover, the quasi-three-dimensional distribution of NPs on the SERS paper greatly enhances the SERS signals within the effective collection volume of a Raman microscope. As a result of the large number of highly effective hot spots and the condensation effect, the hydrophobic SERS paper provides SERS signals with stable and uniform reproducibility throughout the detection area. The limits of detection when using the paper substrates reach the attomolar (10^{-18} M) level, thereby approaching single molecule detection.

Introduction

Paper has been used widely in daily life since its development over 1000 years ago. It has traditionally been used for writing, wrapping, and wiping, yet has found new applications in modern technology—for example, in paper-based electronic devices,[1–3] displays,[4,5] and light emitting diodes.[6,7] In addition, paper-based sensors are of great interest because of their light weight, flexibility, low cost, wide accessibility, and eco-friendliness.[8,9] These outstanding properties make paper a promising alternative to traditional sensing platforms: glass, semiconductors, and plastics. Moreover, there is increasing demand for eco-friendly paper-based biosensors; for example, litmus paper, pregnancy strips, blood glucose dipsticks, and urinalysis dipsticks[10] are already used widely in daily life. Typically, the test paper or the dipstick relies on a color change after the analytes have reacted with the sensor region on the test paper. In a previous study we prepared a colorimetric test paper on photographic paper substrates; that nanoparticle (NP)-containing photographic paper provided a high color contrast before and after binding to analytes.[11] Although colorimetric detection generally provides qualitative information about an analyte, it does not give any detailed insight into the molecule's structure.

Surface-enhanced Raman scattering (SERS) is employed widely in chemical and biological sensing because it can provide abundant molecular information.[12–14] The Raman fingerprint of an analyte reveals the specific chemical bonding of a molecule as well as its symmetry. Therefore, many studies have focused on the development of different types of SERS-active substrates.[15–17] The dominant mechanism of SERS is based on electromagnetic enhancement when analytes are adsorbed on plasmonic metal nanoparticles (NPs) or nanostructures.[12,13] The fabrication of plasmonic nanostructures on paper substrates is desirable for the development of eco-friendly SERS substrates.

Some effort has been devoted to preparing plasmonic NPs on paper substrates.[18–22] For example, Yu *et al.* used inkjet printing to prepare Ag NP spots on chromatography paper and demonstrated the formation of Ag nanoclusters within the spots; coupling between the Ag NPs led to large enhancements in the electric field, thereby achieving a limit of detection (LOD) for rhodamine 6G (R6G) as low as 10^{-11} M.[18] Lee *et al.* employed a dip-coating method to deposit Au nanorods onto a

Department of Materials Science and Engineering, National Taiwan University, No. 1, Sec. 4, Roosevelt Road, Taipei, 10617 Taiwan (R.O.C.).
E-mail: hsuenlichen@ntu.edu.tw; Fax: +886 2 23634562; Tel: +886 2 33664076

†Electronic supplementary information (ESI) available: Background Raman signals of common paper substrates and filter paper before and after coated with a perfluorooctyltrichlorosilane monolayer, SEM images and SERS measurements of Au NP-containing SERS paper. See DOI: 10.1039/c4nr05178e

filter paper; they immersed the filter paper in a Au nanorod solution for two days, allowing the Au nanorods to immobilize onto the paper.[19,20] Unfortunately, such a long incubation time limits the applicability of this method; in addition, many Au nanorods were deposited onto the cellulose fibers deep below the surface, contributing little to the Raman signal enhancement and wasting the Au nanorods. Qu *et al.* used screen-printing for the batch fabrication of disposable SERS arrays, which exhibited high stability and reproducibility, achieving LODs as low as 1.6×10^{-13} M.[21] In contrast to these wet processes, Zhang *et al.* fabricated SERS strips through physical vapor deposition (PVD) of Ag films of certain thicknesses onto rough paper surfaces; the Ag films deposited on the natural wrinkle and fibril structures formed electromagnetic hot spots. These SERS strips exhibited attractive flexibility and hydrophobicity, with LODs for R6G as low as 10^{-10} M.[22]

SERS signals can also be enhanced by concentrating a trace amount of analyte into a small spot on a substrate, taking advantage of hydrophobic effects; the increased number density of the analytes would contribute to the enhanced SERS signals. For such an approach, De Angelis *et al.* used complicated lithography processes to pattern superhydrophobic Si rods; after immobilizing Ag nanoclusters onto the rods, the Ag-decorated superhydrophobic rods concentrated the analytes into a small spot, providing large enhancements in SERS signals, with LODs reaching the attomolar regime.[23] The drawbacks of this approach are the deliberate design of the exquisite superhydrophobic rods and the time-consuming and very expensive fabrication.

Single molecule detection has been achieved using various methods. For example, the Ag-decorated superhydrophobic Si rods described above can concentrate analytes to provide LODs down to the attomolar level. Moreover, complicated plasmonic antennas, such as bow-tie structures, have been fabricated for single molecule detection.[24] Because large electromagnetic fields can form in such antennas, the fluorescence signals of analytes can be enhanced dramatically. Nevertheless, the low number density of hot spots has meant that single molecule detection could be achieved only when the analyte molecules were located coincidentally at the hot spots. In addition, an SPR sensor based on attenuated total reflection (ATR) has been used for single molecule detection after incorporating superparamagnetic particle labels;[25] the binding of magnetic particle clusters to the analytes enhanced the mass and refractive index of the conjugates, thereby allowing trace amounts of analytes to be detected by the SPR sensor. Although other methods, including mechanical cantilevers, capacitance, nanopipettes and nanopores, have been applied recently for single molecule detection,[26–29] they have all required complicated setups and configurations, making such devices poorly suited for use as disposable sensors for daily applications.

In this study, we developed an eco-friendly paper substrate that provides extremely high SERS sensitivity as a result of the formation of NPs through a single-shot laser-induced photothermal effect. This hydrophobic SERS filter paper could efficiently concentrate analytes and, thereby, provide intense Raman signals relative to those found on Si and glass substrates. We found that the micro- and nanoscale hybrid structure of the fibrils within this paper assisted the formation of highly dense NP arrays. Moreover, because the NPs were distributed on the quasi-three-dimensional fibril structures of paper, there were many electromagnetic hot spots within the range of the depth of focus (DOF) of a Raman microscope, effectively contributing to the large intensity of the Raman signals. Accordingly, we could apply this SERS filter paper to the detection of attomolar concentrations of analytes, thereby approaching single molecule detection capability.

Results and discussion

Fig. 1a provides a schematic representation of the use of the laser-induced photothermal effect for the fabrication of NPs on various substrates. Because the physical properties of the substrates (*e.g.*, roughness, morphology, thermal conductivity) would greatly influence the formation of NPs, we selected glass, Si, and paper substrates for comparison. After depositing a Ag or Au film on a Si, glass, or paper substrate, we then illuminated the as-deposited film with several shots from a KrF excimer laser operated at a power density of 125 mJ cm^{-2}. We selected a KrF laser because the extinction coefficients of Ag and Au at 248 nm are 1.19 and 1.95, respectively, with absorption coefficients of 6.04×10^5 and 9.91×10^5 cm^{-1}, respectively.[30] Their strong absorbances in the deep-ultraviolet (DUV) regime would cause these metal films to efficiently convert the incoming power into heat, leading to the formation of metallic NPs. The material properties of the underlying substrates would, however, have a great influence on the formation of such NPs. Silicon is a thermally conducting substrate having a flat surface; glass is typically thermally insulating and also possesses a flat surface; paper comprises micro- and nanoscale fibril structures and has relatively low thermal conductivity. Fig. 1a also compares the formation of NPs on these distinct substrates. For the thermally conducting, flat Si substrate, the deposited metal film was continuous and flat. After several shots of laser illumination, the metal film had broken into a film of some large islands. Further laser illumination led to the formation of some irregular large particles. On the glass substrate, the deposited metal film was also continuous and flat, but only one shot of laser illumination was required to form the film of broken islands, with NP arrays forming after several additional shots of laser illumination. Discontinuous films formed on the paper substrates immediately after deposition, due to their micro- and nanoscale fibril structures. Interestingly, highly dense NP arrays readily formed on the paper substrate after just a single shot of laser light.

Fig. 1b–e display photographic images of particle-containing Si, glass, and paper substrates prepared using different numbers of shots of KrF laser illumination. Highly dense NP arrays formed on the photographic paper and filter paper substrates, as evidenced by the vivid yellow and pink colors that

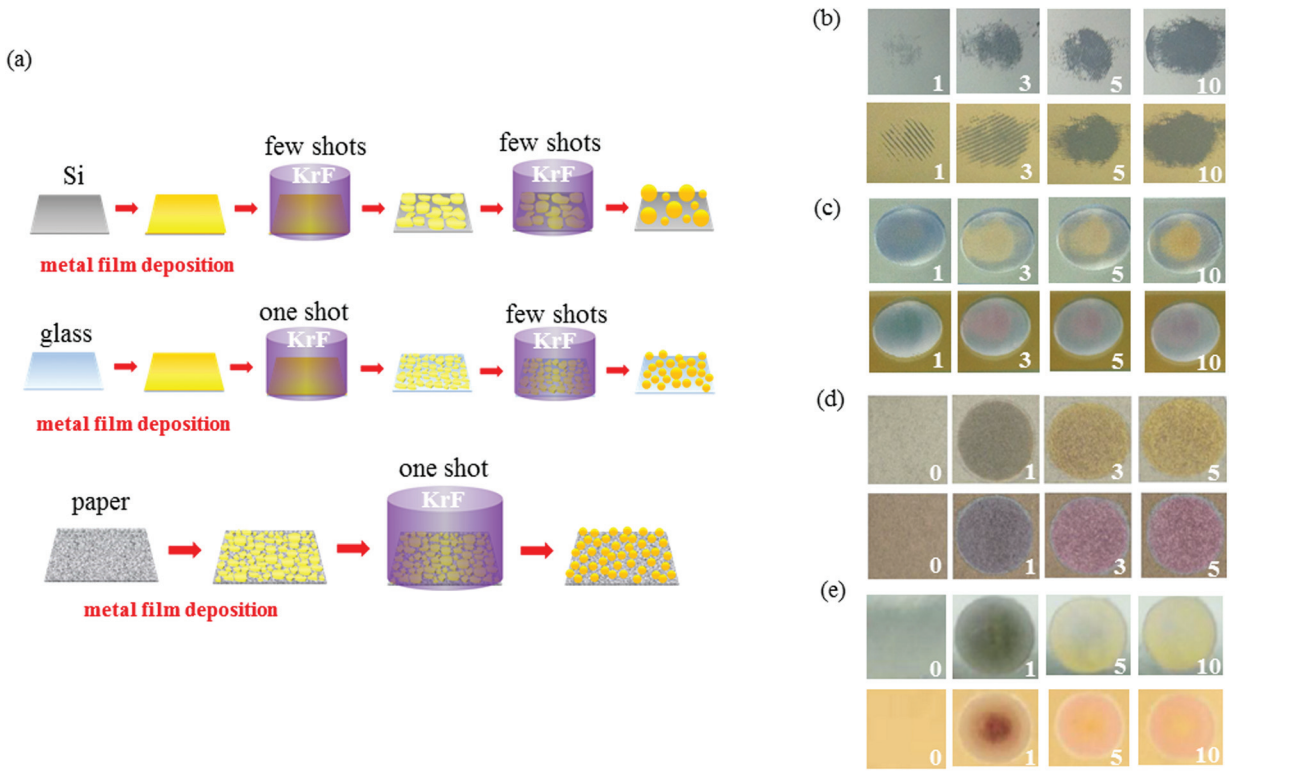

Fig. 1 (a) Schematic representation of the fabrication of NPs on Si (flat, thermally conducting), glass (flat, thermally insulating), and paper (fibrils, thermally insulating) by taking advantage of the laser-induced photothermal effect. (b–e) Photographic images of particle-containing (b) Si, (c) glass, (d) filter paper, and (e) photographic paper prepared using different numbers of shots of KrF laser illumination. Top images: Ag particle-containing substrates; bottom images: Au particle-containing substrates. The numbers indicate the number of laser illumination events.

resulted from the localized surface plasmon resonances (LSPRs) of Ag and Au NPs, respectively. In contrast, the Si substrate did not exhibit such vibrant colors, suggesting that NPs did not form on this substrate. Although the glass substrate displayed the colors of NPs after a few shots of laser illumination, the colors were not as obvious as those on the paper substrates. Therefore, we predicted that the number density of the NPs on the glass was low relative to that on the paper substrates. Our aim for this study was to develop an ultrasensitive SERS paper; we suspected, however, that the background Raman signals from conventional paper substrates would disturb the signals from the analytes and, thereby, decrease the sensitivity of the SERS paper. From an investigation of the background Raman signals of various kinds of paper substrates, we found that filter paper provided the lowest background signals (Fig. S1†).

Fig. 2 displays the surface morphologies and distributions of the Ag NPs that formed on the glass, Si, and filter paper substrates after different numbers of shots of laser illumination. A high density of NPs did not form on the Si substrates until 10 shots of laser irradiation had been applied (Fig. 2d); these large and irregularly shaped particles had a number density of approximately 3 particles per μm^2. For glass substrates, some large particles formed after the first shot, but the maximum density (*ca.* 30 particles per μm^2) was reached after three shots (Fig. 2f). The as-deposited layer of Ag on the filter paper was a discontinuous island film (Fig. 2i). After only a single shot of laser light, this island film had transformed completely into NPs distributed at a high density of approximately 600 particles per μm^2 (Fig. 2j). Upon increasing the number of laser shots, the NPs evaporated or ablated as a result of the excess laser energy, thereby decreasing the particle density (Fig. 2k and l).

We attribute the significantly different morphologies of the NPs formed on these different kinds of substrates to two main factors. The first is the surface morphology of the substrate. The surfaces of Si and glass are very smooth; therefore, films deposited on top of them would be continuous and flat. The formation of NPs is based on nucleation of a melting droplet and its further solidification during the cooling process. To minimize its surface energy, the droplet would shrink into a spherical form, leading to the formation of an NP. No nucleation sites for the melting of droplets are available, however, on a continuous, flat film on a Si or glass substrate; therefore, few NPs formed after the first shot of laser illumination—especially in the case of Si substrates. When some regions of the continuous and flat metal film had ablated under the effects of a few shots of laser illumination, the films of broken islands became nucleation sites for the melting of droplets; accordingly, NPs did form after several shots of laser illumination—for example, after 10 shots for the Si substrate. Nevertheless, the ablation of the metal films during the initial shots

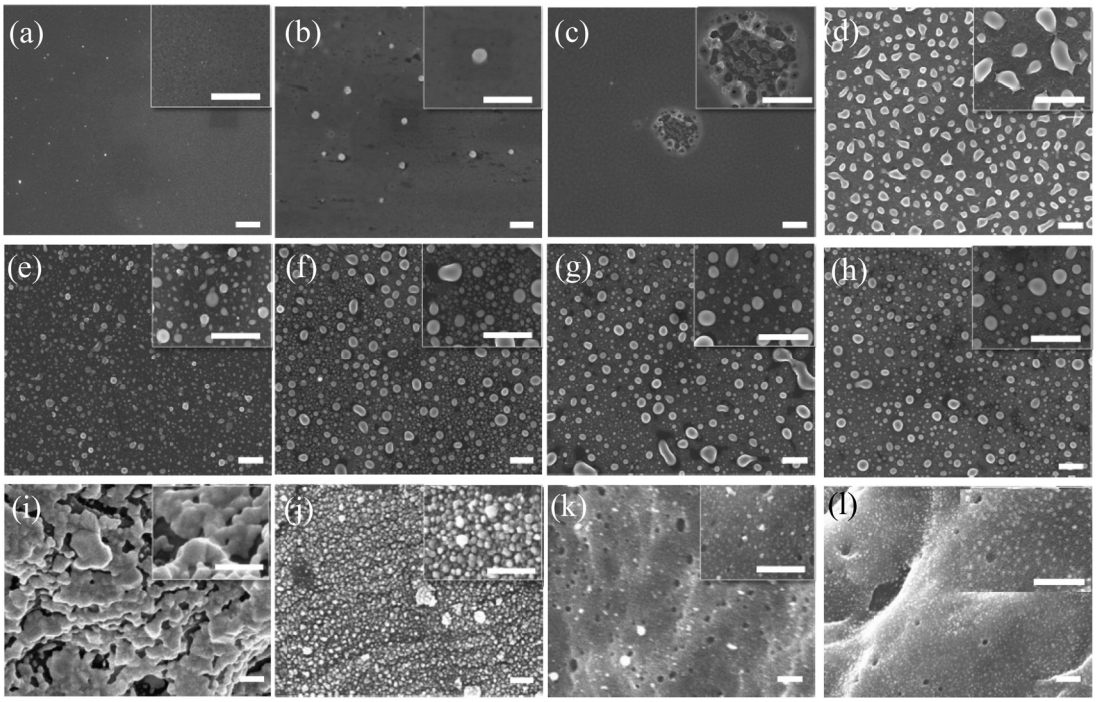

Fig. 2 SEM images of the distributions of Ag NPs formed on (a–d) Si, (e–h) glass, and (i–l) filter paper after different numbers of shots of KrF laser illumination. For Si and glass, the numbers of shots were (from left to right) 1, 3, 5, and 10; for filter paper, the numbers of shots were (from left to right) 0, 1, 3, and 5. Inset: enlarged images of the NPs. Scale bars: (a–h) 1 μm; (i–l) 200 nm.

of laser illumination greatly decreased the density of NPs on these flat substrates.

The second factor playing an important role in the formation of NPs is the thermal conductivity of the substrate. NPs form when the temperature of the metal film exceeds its melting point. Therefore, substrates with high thermal conductivity would rapidly remove heat from the metal films, restricting the formation of NPs. The thermal conductivities of Si, glass, and paper are 142.2, 0.92, and 0.15 W (m K)$^{-1}$, respectively.[31–33] Therefore, in addition to the very few nucleation sites, the local heat generated in a flat, continuous metal film on a Si substrate would rapidly pass through the film itself and to the underlying Si substrate. Thus, the NPs formed only when the number of laser shots exceeded 10, because the film of broken islands increased the number of nucleation sites and inhibited the pathway of heat conduction through the film itself. In contrast, because the thermal conductivity of glass is much lower than that of Si, metallic NPs formed immediately after a single shot of laser illumination. Because of the flat and continuous nature of the metal film on the glass substrate, however, the lack of nucleation sites allowed the heat to also conduct through the continuous metal film, thereby limiting the formation of NPs. Accordingly, only a few large NPs formed on the glass substrate after one shot of laser illumination. After the flat and continuous film on glass had transformed into a film of islands and large NPs, the islands inhibited the conduction of heat and, thereby, functioned as new nucleation sites. Thus, a relatively high density of NPs formed after three shots of laser light, but further irradiation resulted in evaporation or ablation of the NPs, decreasing the density of NPs on the glass substrates.

We found that the application of the laser-induced photothermal effect was very suitable for preparing NPs on paper substrates, which overwhelmed the other substrates for several reasons. First, the micro- and nanoscale roughness of the fibril structures caused the metal films deposited on paper substrates to be discontinuous films of irregular islands, rather than flat and continuous films (Fig. 2i). The discontinuous and irregular islands acted as multiple nucleation sites and suppressed the conduction of heat through both the paper substrate and the film itself. Notably, the low thermal conductivity of paper [0.15 W (m K)$^{-1}$] allowed the photothermal effect to be much more obvious on the paper substrate. Accordingly, we found that a great quantity of NPs of uniform size formed on the filter paper substrate after only a single shot of laser illumination. Unlike the NPs that formed on the Si and glass substrates, the NPs on the filter paper substrate were of uniform size and high density, contributing to a great enhancement in electric field intensity everywhere on the filter paper. Fig. S2† reveals that the same method could be used to also prepare Au NPs of uniform size and high density on filter paper substrates.

Fig. 3 summarizes the size distributions of Ag NPs formed on different substrates after laser illumination. Here, we used SEM images to estimate the size distributions within a 10×10 μm^2 area. For the Si substrate, only large particles had formed after 10 shots of laser illumination. Notably, the particles that formed on this substrate had a broad distribution of

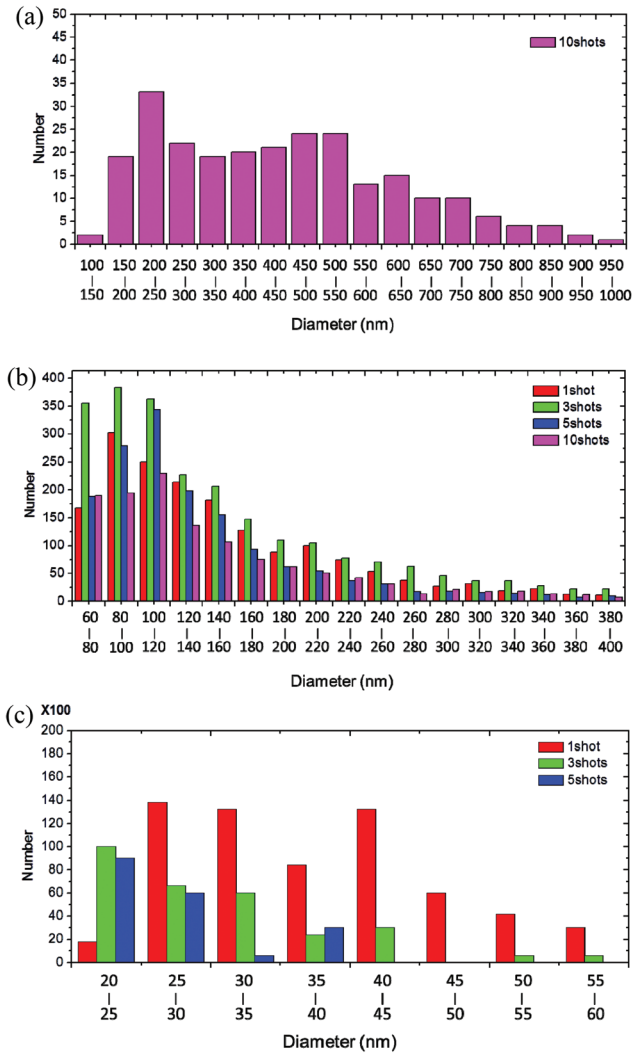

Fig. 3 Particle size distribution within a 10 × 10 μm^2 area of Ag NPs formed on (a) Si, (b) glass, and (c) filter paper.

sizes, with a large standard deviation (STD; close to 190 nm); in addition, these large particles possessed relatively irregular shapes. In contrast, the NPs that formed on the glass substrate after a single shot of laser light had sizes distributed from 60 to 400 nm; most of these NPs had sizes of less than 200 nm, with some larger particles. The density of NPs reached its maximum after three shots, with most of the NPs having sizes of less than 160 nm, although some large particles were still observed. After five shots of laser illumination, the density of NPs decreased, with most of them having sizes of less than 160 nm as well. After three shots of laser illumination, the STD of the sizes of the NPs was approximately 76 nm. Notably, the STDs of the sizes were large for the NPs formed on the Si and glass substrates. Thus, neither the smooth, thermally conducting Si surface nor the smooth, poorly thermally conducting glass substrate was suitable for the formation of NPs through this approach taking advantage of the photothermal effect. In addition, the nucleation sites formed only after these flat films had broken in a non-uniform manner under the laser illumination. Therefore, the NPs that formed on the Si and glass substrates both featured irregular shapes, low densities, and broad size distributions.

In contrast, metallic NPs formed readily on filter paper substrates. The density of NPs reached its maximum after a single shot of laser illumination. In addition, the density of the NPs formed on filter paper was much higher than those on the other two substrates. The number density of the NPs decreased gradually, however, after applying additional shots of laser illumination, with only small NPs (<40 nm) remaining. The size distribution of the NPs formed on the filter paper substrate ranged from a few to tens of nanometers. The average size of the NPs on the filter paper substrate after a single shot of laser illumination was approximately 37 ± 9 nm; it decreased to 30 ± 8 nm after three shots and 26 ± 5 nm after five shots. The STD of the NP size was much lower than those of the NPs formed on the Si and glass substrates. The density and average size of these NPs confirmed our proposition that the films of discontinuous islands on the rough and fibrous paper substrates promoted nucleation and prevented the dissipation of thermal energy.

We made these NP-containing substrates hydrophobic by coating them with perfluorooctyltrichlorosilane and then placed a droplet of an analyte solution onto the hydrophobic SERS substrates. Because of the large contact angles of the substrates, the analytes concentrated into small spots during the drying process, assisting the detection of trace amounts of the analytes. Through this concentrating effect, low volumes of analyte solutions could provide large signal intensities. We compared the SERS performance of the hydrophobic NP-containing Si, glass, and filter paper substrates. From the SEM images in Fig. 2, we selected NP-containing Si, glass, and filter paper substrates that had been fabricated under ten, three, and one shot laser illumination, respectively, because they featured the densest Ag NPs. Fig. 4 presents SERS spectra of 10^{-6} M R6G that had been dried on these NP-containing substrates. The SERS performance of the filter paper substrates, featuring highly dense and uniform NPs, was superior to that of the other two substrates, presumably because of the

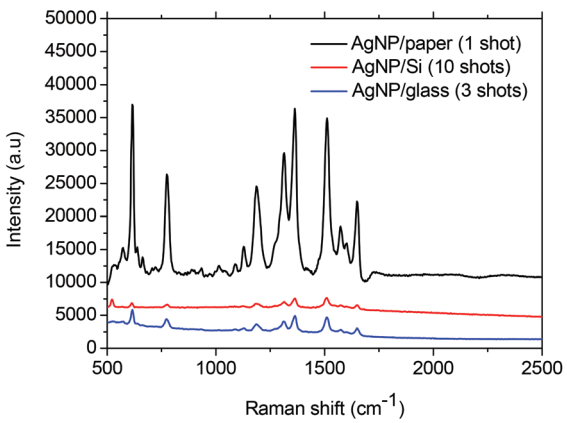

Fig. 4 SERS spectra of 20 μL R6G (10^{-6} M) droplets that had been dried on various hydrophobic SERS substrates.

low densities of NPs on the surfaces of the glass and Si. Note that the perfluorooctyltrichlorosilane coating did not display any noise signals in the background (Fig. S3†). In addition, the filter paper substrates presenting Au NPs also provided large SERS enhancement (Fig. S2 and S4†).

In addition to the high density of NP arrays, most of the NPs formed in the filter paper substrate were positioned on the surfaces of the top fibril structures. We can consider these NPs to have a "quasi-3D" distribution; such an array of hot spots might efficiently enhance the Raman signal intensities within the collection volume of a Raman microscope. In previous studies, the collection volume of a Raman microscope was estimated to be that of a cylinder having a diameter equal to the spot size of the laser beam, in turn depending on the numerical aperture (NA) of the objective lens.[34–36] The height of the cylinder (probe length) was determined by moving the sample out of the focus plane vertically and then recording the Raman peak intensity at each position. The probe length was the ratio between the Raman intensities integrated over all positions and the maximum intensity at the focal plane. The Raman peak intensity would, however, decay dramatically at positions far from the focal plane. The DOF of a microscope is the range of distances in object space for which object points are imaged with acceptable resolution relative to the focal plane. Therefore, we believe that a large proportion of the Raman signals arose from a collection volume within the DOF of the microscope. The DOF of a Raman microscope can be estimated using the equation:[37]

$$\mathrm{DOF} = \frac{n\lambda}{2\mathrm{NA}^2} \quad (1)$$

where n is the refractive index of the object space medium, λ is the wavelength of incident light, and NA is the numerical aperture of the objective lens. Table 1 summarizes the DOFs of generally used objective lenses.

Although the DOF is typically smaller than the probe length of the collection volume, the signals acquired within the DOF would dominate the overall intensity. Therefore, we should consider the DOF of a Raman microscope when we have a 3D distribution of hot spots. The DOF of a Raman microscope is typically in the range from a few hundred nanometers to a few micrometers; this range is similar to that of the sizes of the fibril structures on filter paper. For example, the DOF of a 10× objective lens (5.1 μm) is similar to the size of microscale fibers, whereas the DOF of a 100× objective lens is close to the size of nanoscale fibers. Therefore, most of the NPs formed on the fibril structures of filter paper substrates were located densely within the DOF range.

Table 1 Depth of focus (DOF) and spot size in SERS measurements under He–Ne laser (633 nm) excitation

Objective lens	Numerical aperture (NA)	DOF (μm)	Spot size (μm)
10×	0.25	5.1 (microscale fibers)	3.0
20×	0.4	2.0	1.9
40×	0.65	0.75	1.2
60×	0.85	0.45	0.9
100×	0.95	0.35 (nanoscale fibers)	0.8

We suspect that a quasi-3D distribution of hot spots would enhance the Raman signals even more than those in two-dimensional (2D) or 3D distributions. In a common flat substrate (*e.g.*, glass, Si), the hot spots are distributed in a 2D manner; therefore, we found that the SERS signals had the greatest intensity when the focal plane was consistent with the plane on which the hot spots were located. Although Raman scattering in the focal plane dominated the measured Raman intensity, scattering within the DOF range remained an important part of the measured signal. 3D distributions of NPs have also been proposed—for example, for NP-containing paper substrates fabricated using an immersion method.[19,20,38] By immersing a paper substrate into a colloidal NP solution for a long duration, the NPs would attach to the fibers throughout the paper substrate; the resulting hot spots would be distributed not only on the surface but also deep within the paper.

The quasi-3D distribution of hot spots formed in response to the laser-induced photothermal effect on the paper substrate was a better SERS substrate than was a corresponding 3D distribution formed through the immersion method. First of all, the immersion method did not provide as high a density of NPs as did the laser-induced photothermal effect; this lower density of NPs resulted in weaker SERS performance. Second, the thickness of a sheet of paper (several hundred micrometers) is typically much larger than the DOF of a Raman microscope; therefore, any NPs (hot spots) located outside the DOF would not assist in increasing the measured Raman intensity. In other words, the immersion method would waste the NP solution because most of the NPs in the paper would be located outside the DOF. On the other hand, the laser-induced photothermal effect produced NPs on and beneath the paper surface within a distribution of only a few micrometers; therefore, most of the NPs (hot spots) were within the DOF and could contribute efficiently to the enhancement of the Raman signals.

We used the three-dimensional finite-difference time domain (3D-FDTD) method to simulate the electric field intensity of hot spots distributed in 2D, quasi-3D, and 3D arrays. In performing the simulations, we focused a plane wave through a lens to simulate a real Raman microscope setup. In Fig. 5, the direction of incident light is indicated by a white arrow, with the configurations of the lens, substrates, and NPs outlined by white solid lines. The colors in the images are related to different magnitudes of the electric field amplitude. When the NPs were distributed in a 2D manner, coupling between adjacent NPs led to a great enhancement in the electric field (Fig. 5b), but a monolayer of hot spots did not enhance the Raman signals the most within the DOF range. In contrast, the quasi-3D distribution of NPs provided many hot spots within the DOF (Fig. 5c, region between the two yellow dashed lines). The electric field was enhanced dramatically between adjacent NPs, with the density of hot spots being larger than that in the case of a 2D distribution. In addition, we also observed

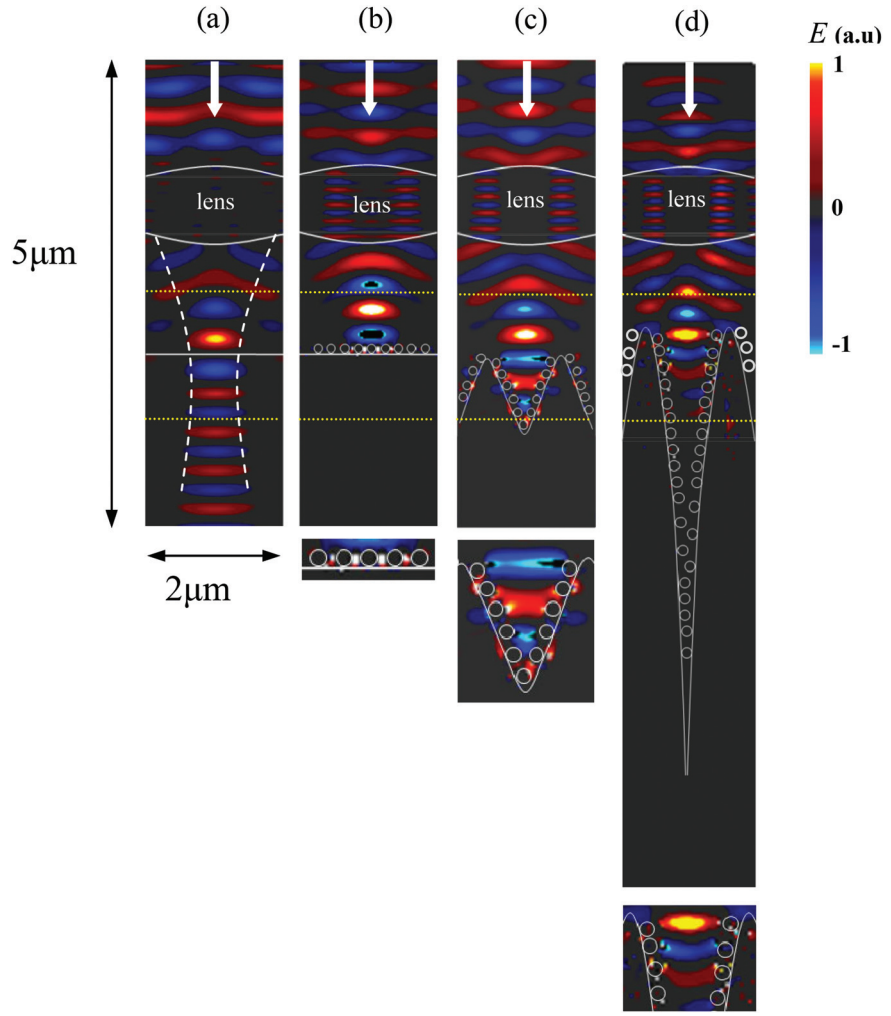

Fig. 5 3D-FDTD simulations of electric field amplitudes on (a) a flat SiO_2 substrate and (b–d) Ag NPs distributed in (b) 2D, (c) quasi-3D, and (d) 3D arrays. Because incident light was focused by a lens, only the NPs on the focal plane and within the DOF range contributed effectively to the electromagnetic hot spots. The bottom images in (b–d) display enlarged views of the electromagnetic hot spots. The direction of incident light is indicated by a white arrow; the configurations of the lens, substrates, and NPs are outlined by white solid lines. The white dashed line in (a) demonstrates the focusing of incident light; the regions between the two yellow dashed lines in (a–d) indicate the DOF.

coupling between these hot spots, leading to further enhancement in the electric field. Accordingly, the Raman signals were excited predominantly within these hot spots in the quasi-3D distribution. The density of hot spots in the 3D distribution of NPs (Fig. 5d)—an arrangement typically found in SERS-active substrates prepared through immersion—was lower than those in the 2D and quasi-3D distributions. Therefore, the electric field inside this 3D configuration was weaker. In addition, for a 3D distribution of NPs, the bottom NPs could not interact with the incident light because of the large scattering and absorption of light from the upper NPs. Accordingly, the bottom NPs and those outside the DOF did not contribute effectively to the SERS measurement. As indicated in the simulation images, a high density of NPs located outside the DOF would not enhance the electric field intensity nearby. When considering the SERS efficiency, the ease of fabrication, and material savings, we believe that NP-containing filter paper substrates prepared through a single shot of laser light, taking advantage of the laser-induced photothermal effect, are the most practical SERS substrates.

As described above, the morphology of a substrate greatly affects the formation of NPs. Therefore, we suspected that filter paper substrates with different pore sizes would also influence the formation of NPs. Accordingly, we compared three kinds of filter paper, featuring pore sizes of 20, 8, and 2.5 μm. In general, the pore size of filter paper determines the average size of the impurities that would be blocked. For example, a filter paper having a pore size of 20 μm would block impurities having an average size of greater than 20 μm. Therefore, we suspected that the distribution of NPs would be different when formed on filter papers possessing different pore sizes. Fig. 6a–c display SEM images of the NPs formed on the filter papers of different pore sizes of a single shot of laser illumination; the insets present images of the blank filter

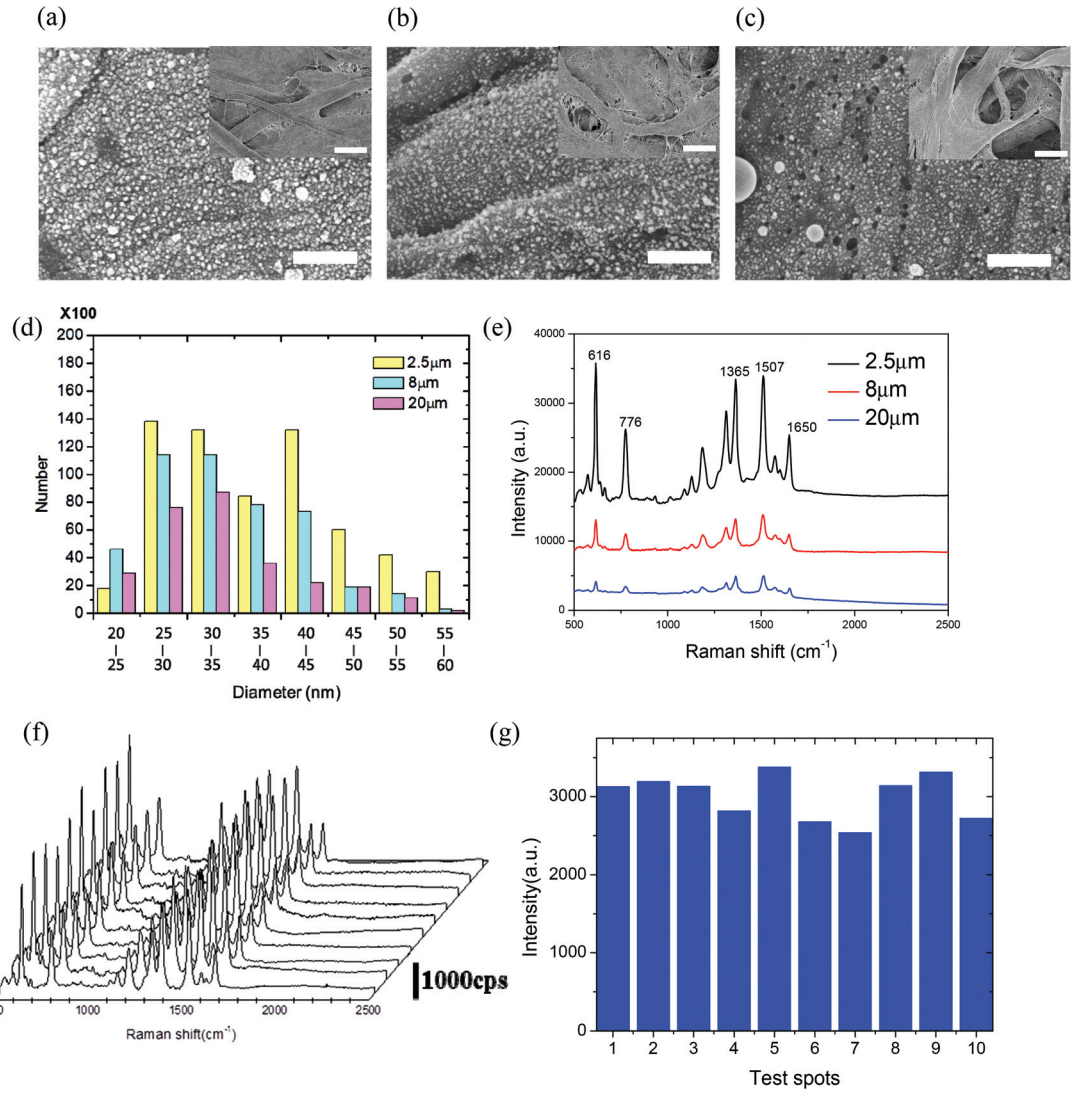

Fig. 6 (a–c) SEM images of Ag NPs formed on filter papers having pore sizes of (a) 2.5, (b) 8, and (c) 20 μm (scale bars: 500 nm). Inset: morphologies of blank filter papers of various pore sizes (scale bars: 25 μm). (d) NP size distributions within a 10 × 10 μm^2 area for filter papers of various pore sizes. (e) SERS spectra of 20 μL R6G (10^{-6} M) dried on Ag NP-containing SERS filter papers of various pore sizes. (f) Reproducibility of SERS spectra of R6G collected at 10 randomly selected spots on the same SERS filter paper (pore size: 2.5 μm). (g) Intensity of the signal at 1507 cm^{-1} of R6G collected at 10 randomly selected spots on the same SERS filter paper.

papers. The NP arrays formed on the filter paper featuring a pore size of 2.5 μm had a higher packing density than those formed on the other two filter papers. The surface coverages of the NPs formed on the filter papers having pore sizes of 2.5, 8, and 20 μm, estimated from the SEM images, were approximately 70, 50, and 30%, respectively. Furthermore, Fig. 6d displays the size distributions of the NPs on the filter papers of various pore sizes; in each case, most of the NPs had diameters of approximately 25–35 nm, suggesting that the mechanism of formation of the NPs was similar on the three filter papers. Although the filter papers featured different pore sizes, the morphologies and thermal conductivities of their single fibers—the factors influencing the nucleation of NPs—remained almost identical, thereby resulting in NPs of similar particle sizes. Nevertheless, the pore size would influence the density of the NPs. When we deposited the metal film onto a filter paper featuring a larger pore size, some of the metal films would be deposited through the pores and onto fibers deep below the surface. Accordingly, the surface coverage of the metal film decreased, thereby decreasing the density of NPs within the DOF of the Raman microscope and, subsequently, decreasing the contribution to the Raman signals.

We compared the SERS spectra of R6G (from a solution having a concentration of 10^{-6} M) adsorbed on Ag NP-containing filter paper substrates featuring different pore sizes (Fig. 6e). The NPs on these filter paper substrates were all formed through a single shot of KrF laser illumination. The SERS signals on the NP-containing filter paper having a pore size of 2.5 μm had the strongest intensity, decreasing significantly upon increasing the pore size of the filter paper. This

phenomenon was presumably related to the density of NPs, as described above. For a filter paper having a smaller pore size, the as-fabricated NPs would cover the surface to a greater extent, leading to a dramatic enhancement in SERS signals. When the pore size increased, more NPs formed beneath the range of the DOF, thereby decreasing the intensity of the SERS signals. Notably, because the NPs were distributed densely throughout the SERS filter paper featuring a pore size of 2.5 μm, this substrate provided highly reproducible SERS signals. When we collected the SERS signals of R6G from 10 randomly selected spots on the SERS filter paper featuring a pore size of 2.5 μm (Fig. 6f), the intensity of the signals remained nearly identical. Fig. 6g plots the spot-to-spot intensity of the characteristic signal of R6G at 1507 cm^{-1} measured at different points; the standard deviation of the signal intensity was less than 10%. These findings are consistent with NPs having formed uniformly with a high density on the filter paper as a result of the laser-induced photothermal effect. The high reproducibility of these SERS signals implies that SERS filter paper substrates would be potentially useful analytical tools for quantitative detection.

As described above, the NP-containing filter paper substrate having a pore size of 2.5 μm, formed by applying a single shot of laser illumination, had the most intense electric field enhancement. Therefore, we employed it to test the LOD of the NP-containing filter paper substrates. We placed 20 μL droplets of R6G solutions of various concentrations on the SERS filter paper and then dried them. The SERS spectra in Fig. 7a reveal that the Raman signals of R6G on the SERS filter paper were enhanced dramatically, with detection at a concentration as low as 10^{-15} M R6G, where a 20 μL droplet would contain approximately 12 040 R6G molecules. When the 20 μL droplet dried, it concentrated the R6G molecules into an area of approximately 3 mm^2; therefore, on average, there would be only 0.28 R6G molecules within the spot size (Table 1: diameter, 3 μm; 10× objective lens). This less-than-unity value indicates that the R6G molecules were not distributed uniformly within the dried area. Mapping of the signals over the area would be necessary to detect such a trace amount of analyte. Nonetheless, because the NPs were formed densely and uniformly on the SERS filter paper, the trace R6G molecules would certainly be located around the hot spots, even if their distributions were non-uniform. As a result, the SERS signals of R6G at 10^{-15} M were readily detected when using our SERS filter paper as the substrate.

To further test the SERS performance of this SERS filter paper for the detection of other analytes, we dried 20 μL droplets of 4-ATP solutions of various concentrations onto the Ag NP-containing SERS filter paper. Because of the high density of hot spots within the DOF of the Raman microscope, we could detect 4-ATP at an attomolar (10^{-18} M) concentration. Furthermore, we calculated that only approximately 12 molecules of 4-ATP would be present in a 20 μL droplet at an attomolar concentration [10^{-18} (mol L^{-1}) × 6.02 × 10^{23} (molecules per mol) × 20 × 10^{-6} (L)]. As mentioned above, these molecules would not be distributed uniformly within the dried area at

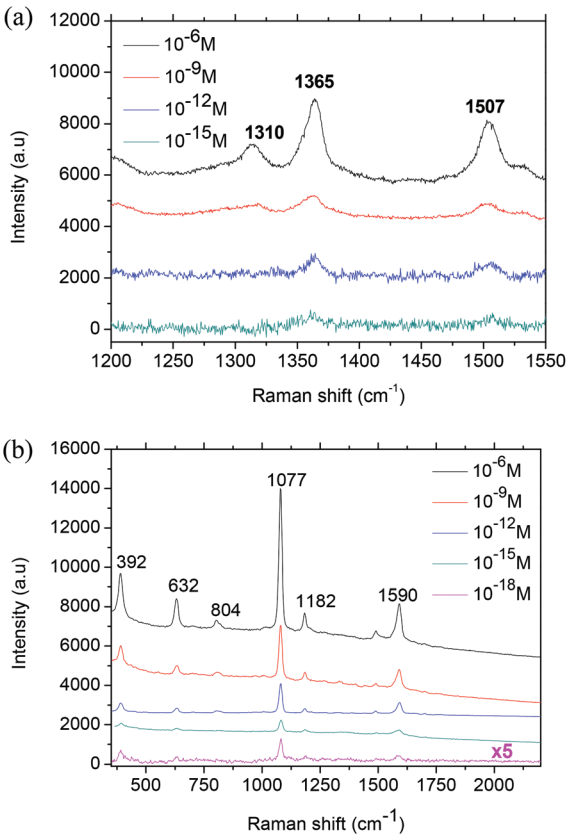

Fig. 7 SERS spectra of various concentrations of (a) R6G and (b) 4-ATP dried on Ag NP-containing SERS filter paper, demonstrating attomolar detection ability.

such a trace level. Again, we detected the SERS signals of 4-ATP by mapping the signals. We believe that the SERS signals from 20 μL droplets of R6G (10^{-15} M) and 4-ATP (10^{-18} M) were recorded (Fig. 7a and b, respectively) from only a few molecules, according to our estimates above. Therefore, the SERS filter paper developed in this study was a highly sensitive substrate with detection capability approaching that of the single molecule. We could also use the laser-induced photothermal effect to fabricate other types of metal NPs on filter paper. The Au NP-containing SERS filter paper that we obtained using this method also demonstrated ultrasensitive detection capability, down to attomolar concentrations (Fig. S4†). Notably, in many previous studies, approaching single molecule detection could be achieved only when employing very complicated processes or devices.[23–29]

Conclusions

In summary, we have developed an ultrasensitive and eco-friendly SERS filter paper by taking advantage of the DUV laser-induced photothermal effect. Unlike the situation on common Si and glass substrates, the rough fibril morphology of paper substrates assisted the formation of NPs. The metal films deposited on filter paper featured a morphology of

broken islands, in contrast to the flat films formed on the Si and glass. The films of discontinuous islands provided many nucleation sites for NPs and prevented the thermal energy from conducting and dissipating. Therefore, NPs formed readily on filter paper substrates after just a single shot of laser illumination. We found that a quasi-3D distribution of NPs functioned as a better SERS substrate relative to either a 2D or 3D array. Only the NPs located within the DOF were effective hot spots. Thus, the SERS filter paper, which featured a large quantity of NPs (hot spots) within the DOF, provided SERS signals of the highest intensities. The pore size of the filter paper substrate influenced the density of NPs and, thus, the SERS performance; indeed, the filter paper featuring the smallest pores had the densest NPs and the strongest SERS signals. Because of the large number of hot spots within the DOF and the condensation effect, the reproducibility of the SERS signals on the hydrophobic SERS filter paper remained stable and uniform throughout the detection area. These characteristics allowed the SERS filter paper featuring pores of 2.5 μm to achieve LODs down to the attomolar level—approaching single molecule detection after using a simple fabrication procedure.

Methods

Fabrication of NP-containing SERS substrates

A 30 nm-thick Ag or Au film was deposited onto Si, glass, or filter paper (Whatman® no. 42) by operating a sputtering system at a rate of 3 Å s^{-1}. For comparison, a 15 nm-thick Ag or Au film was deposited onto commercial photographic paper featuring a water-resistant coating, according to the optimal procedure in our previous study.[11] These substrates were then illuminated with various numbers of shots from a KrF excimer laser (λ: 248 nm; pulse width: 20 ns; power density: 125 mJ cm^{-2}). After the Ag or Au NPs had formed, the NP-containing substrates were made hydrophobic by evaporating perfluorooctyltrichlorosilane onto the substrates. Filter papers featuring pore sizes of 2.5 μm (Whatman® no. 42), 8 μm (Whatman® no. 40), and 20 μm (Whatman® no. 41) were also applied for comparison. The morphologies of the filter paper and the NP-containing substrates were examined through scanning electron microscopy (SEM; Hitachi S-4700I).

SERS measurement

A 20 μL droplet of R6G (Sigma-Aldrich) or 4-aminothiophenol (ChemService) was placed on a hydrophobic NP-containing SERS substrate. SERS measurement was performed using a commercial confocal Raman microscope (WITec, alpha 300 R). The excitation laser line was that from a He–Ne laser having a wavelength of 633 nm and a power of 34 mW. A 10× objective lens was used; the integration time was 5 s.

Acknowledgements

We thank the Ministry of Science and Technology, Taiwan, for supporting this study under contracts MOST-103-2221-E-002-041-MY3 and MOST-103-2221-E-002-092-MY3. We also thank Prof. Lon Alex Wang from Graduate Institute of Photonics and Optoelectronics at National Taiwan University for providing the KrF excimer laser and technical assistance.

Notes and references

1 D. Tobjörk and R. Österbacka, *Adv. Mater.*, 2011, **23**, 1935–1961.
2 U. Zschieschang, T. Yamamoto, K. Takimiya, H. Kuwabara, M. Ikeda, T. Sekitani, T. Someya and H. Klauk, *Adv. Mater.*, 2011, **23**, 654–658.
3 F. Eder, H. Klauk, M. Halik, U. Zschieschang, G. Schmid and C. Dehm, *Appl. Phys. Lett.*, 2004, **84**, 2673–2675.
4 J. Shah and R. M. Brown, Jr., *Appl. Microbiol. Biotechnol.*, 2005, **66**, 352–355.
5 D. Y. Kim and A. J. Steckl, *ACS Appl. Mater. Interfaces*, 2010, **2**, 3318–3323.
6 G. Amin, S. Zaman, A. Zainelabdin, O. Nur and M. Willander, *Phys. Status Solidi RRL*, 2011, **5**, 71–73.
7 M. Y. Soomro, S. Hussain, N. Bano, I. Hussain, O. Nur and M. Willander, *Phys. Status Solidi A*, 2013, **210**, 1600–1605.
8 Y. Ma, H. Li, S. Peng and L. Wang, *Anal. Chem.*, 2012, **84**, 8415–8421.
9 J. W. Han, B. Kim, J. Li and M. Meyyappan, *J. Phys. Chem. C*, 2012, **116**, 22094–22097.
10 R. Pelton, *TrAC, Trends Anal. Chem.*, 2009, **28**, 925–942.
11 S. C. Tseng, C. C. Yu, D. H. Wan, H. L. Chen, L. A. Wang, M. C. Wu, W. F. Su, H. C. Han and L. C. Chen, *Anal. Chem.*, 2012, **84**, 5140–5145.
12 M. Fleischmann, P. J. Hendra and A. J. McQuillan, *Chem. Phys. Lett.*, 1974, **26**, 163–166.
13 A. Campion and P. Kambhampati, *Chem. Soc. Rev.*, 1998, **27**, 241–249.
14 E. C. Le Ru, E. Blackie, M. Meyer and P. G. Etchegoin, *J. Phys. Chem. C*, 2007, **111**, 13794–13803.
15 N. A. Hatab, C. H. Hsueh, A. L. Gaddis, S. T. Retterer, J. H. Li, G. Eres, Z. Zhang and B. Gu, *Nano Lett.*, 2010, **10**, 4952–4955.
16 M. Chirumamilla, A. Toma, A. Gopalakrishnan, G. Das, R. P. Zaccaria, R. Krahne, E. Rondanina, M. Leoncini, C. Liberale, F. De Angelis and E. Di Fabrizio, *Adv. Mater.*, 2014, **26**, 2353–2358.
17 X. Li, Y. Zhang, Z. X. Shen and H. J. Fan, *Small*, 2012, **8**, 2548–2554.
18 W. W. Yu and I. M. White, *Anal. Chem.*, 2010, **82**, 9626–9630.
19 C. H. Lee, M. E. Hankus, L. Tian, P. M. Pellegrino and S. Singamaneni, *Anal. Chem.*, 2011, **83**, 8953–8958.
20 C. H. Lee, L. Tian and S. Singamaneni, *ACS Appl. Mater. Interfaces*, 2010, **2**, 3429–3435.

21 L. L. Qu, D. W. Li, J. Q. Xue, W. L. Zhai, J. S. Fossey and Y. T. Long, *Lab Chip*, 2012, **12**, 876–881.

22 R. Zhang, B. B. Xu, X. Q. Liu, Y. L. Zhang, Y. Xu, Q. D. Chen and H. B. Sun, *Chem. Commun.*, 2012, **48**, 5913–5915.

23 F. De Angelis, F. Gentile, F. Mecarini, G. Das, M. Moretti, P. Candeloro, M. L. Coluccio, G. Cojoc, A. Accardo, C. Liberale, R. P. Zaccaria, G. Perozziello, L. Tirinato, A. Toma, G. Cuda, R. Cingolani and E. Di Fabrizio, *Nat. Photonics*, 2011, **5**, 682–687.

24 A. Kinkhabwala, Z. Yu, S. Fan, Y. Avlasevich, K. Mullen and W. E. Moerne, *Nat. Photonics*, 2009, **3**, 654–657.

25 S. Krishnan, V. Mani, D. Wasalathanthri, C. V. Kumar and J. F. Rusling, *Angew. Chem., Int. Ed.*, 2011, **50**, 1175–1178.

26 S. W. Stahl, E. M. Puchner and H. E. Gaub, *Rev. Sci. Instrum.*, 2009, **80**, 073702.

27 S. Loyprasert, M. Hedström, P. Thavarungkul, P. Kanatharana and B. Mattiasson, *Biosens. Bioelectron.*, 2010, **25**, 1977–1983.

28 M. Karhanek, J. T. Kemp, N. Pourmand, R. W. Davis and C. D. Webb, *Nano Lett.*, 2005, **5**, 403–407.

29 W. W. Li, L. Gong and H. Bayley, *Angew. Chem., Int. Ed.*, 2013, **52**, 4350–4355.

30 E. D. Palik, *Handbook of Optical Constants of Solids*, Academic Press, INC., San Diego, 1985.

31 H. R. Shanks, P. D. Maycock, P. H. Sidles and G. C. Danielson, *Phys. Rev.*, 1963, **130**, 1743–1748.

32 D. Mann, R. E. Field and R. Viskanta, *Wärme Stoffübertragung*, 1992, **27**, 225–231.

33 R. Lopatkiewicz, Z. Nadolny and P. Przybylek, in 2012 IEEE 10th International Conference on the Properties and Applications of Dielectric Materials, Bangalore, India, July 24–28, 2012.

34 Y. Chu, M. G. Banaee and K. B. Crozier, *ACS Nano*, 2010, **4**, 2804–2810.

35 Y. S. Hu, J. Jeon, T. J. Seok, S. Lee, J. H. Hafner, R. A. Drezek and H. Choo, *ACS Nano*, 2010, **4**, 5721–5730.

36 H. Y. Wu, C. J. Choi and B. T. Cunningham, *Small*, 2012, **8**, 2878–2885.

37 R. H. Webb, *Rep. Prog. Phys.*, 1996, **59**, 427–471.

38 Y. H. Ngo, D. Li, G. P. Simon and G. Garnier, *Langmuir*, 2012, **28**, 8782–8790.